Rev. Roum. Sci. Techn.– Électrotechn. et Énerg.
Vol. **71**, *2*, pp. 241–246, Bucarest, 2026

NONLINEAR DYNAMIC ANALYSIS OF TRANSFORMER SATURATION INDUCED BY SUBSYNCHRONOUS RESONANCE

NEEVATIKA VERMA[1,2], NARENDRA KUMAR [1]

Keywords: Subsynchronous Resonance (SSR); Transformer saturation; Series compensation; Flux dynamics; Magnetizing current; Post-fault transients.

This paper presents a novel investigation into the influence of post-fault subsynchronous resonance (SSR) on transformer flux dynamics and saturation behavior. A theoretical framework is established to examine resonance conditions in fixed-series-compensated transmission lines using frequency-domain impedance analysis, identifying electrical resonance points that can induce subsynchronous excitation. A nonlinear flux-voltage integral model is developed and implemented in MATLAB/Simulink to simulate transformer response under fault-clearing scenarios. Results reveal that the SSR-induced voltage recovery—particularly at 10 Hz—can drive the core flux well beyond the saturation knee, reaching up to 1.89 pu. The corresponding magnetizing current exhibits 20 Hz modulation, generating intermodulation sidebands at 40 Hz, 80 Hz, 110 Hz, and 130 Hz. Comparative analysis shows that series compensation significantly amplifies flux excursions and spectral distortion, confirming the role of transformer saturation as a nonlinear resonance amplifier. These findings underscore the importance of incorporating nonlinear transformer modeling into SSR studies for accurate assessment and mitigation in modern compensated power systems.

1. INTRODUCTION

With rising electricity demand, integrating renewable energy into existing grids has become essential. To enhance power transfer and stability, compensation techniques such as shunt capacitors, STATCOM, and series capacitors (FSC, TCSC) are widely used [1,2]. However, series compensation can introduce Subsynchronous Resonance (SSR), where energy exchange between the network and rotating machinery at subsynchronous frequencies leads to oscillations, causing stability issues and potential damage to turbine-generator shafts and other equipment [3].

Since the 1970s, SSR has been extensively studied, especially for its impact on turbine-generator torsional modes and more recently, on inverter-based renewable energy systems [3,4]. However, the effect of SSR on power transformers, particularly magnetic core saturation during SSR conditions, remains underexplored.

Subsynchronous voltage and current oscillations caused by SSR can drive power transformers into their nonlinear operating region, resulting in magnetic core saturation [5]. This phenomenon is especially critical during fault-clearing events or transient operating conditions, where sharp voltage excursions coincide with subsynchronous frequencies. Saturation of the transformer core under such conditions can lead to waveform distortion, harmonic injection, flux demodulation, and maloperation of protection devices [6]. Yet, most SSR-focused studies continue to model transformers as linear components, thereby neglecting their nonlinear magnetic behavior and its potential feedback into the SSR dynamics.

Existing studies on transformer saturation mainly address mechanisms unrelated to SSR. Some focus on DC bias and harmonic instability in HVDC systems, where core saturation arises from unidirectional currents [7]. Others examine current transformer saturation due to decaying DC components during faults, which differs from SSR-induced effects [8]. Additional work considers geomagnetically induced currents (GICs) during solar storms, which introduce low-frequency quasi-DC components that saturate cores [9], but under conditions unlike those in series-compensated AC systems. Similarly, studies on flux walking in high-frequency transformers (*e.g.*, dual-active-bridge converters) operate in entirely different frequency domains [10]. Moreover, impedance-based SSR analyses rarely account for transformer saturation [11].

This paper addresses the gap by investigating transformer core saturation under SSR in a series-compensated system. A nonlinear transformer model is developed and analyzed in a time-domain framework using MATLAB/Simulink. The main contributions are:

- Identification of resonance frequencies that increase the risk of transformer core saturation in series-compensated systems.
- Modeling and simulation of nonlinear transformer behavior during SSR events using MATLAB/Simulink.
- Spectral analysis reveals sidebands and harmonic intermodulation due to 20 Hz modulation of magnetizing current.
- Demonstration that series compensation amplifies flux excursions and nonlinear distortion after faults.

The paper is organized as follows: Section 2 reviews SSR theory; Section 3 describes the study system; Section 4 presents the system modeling; Section 5 discusses the results; and Section 6 concludes with key contributions.

2. SSR MECHANISM AND ITS IMPACT ON NETWORK COMPONENTS

Theoretical aspects of SSR are described in [12]. Assuming negligible line resistance, the power transfer capability can be expressed as:

$$P = \frac{V_S . V_T}{X_T} \sin\delta. \tag{1}$$

Here, P is the transmitted power, V_S and V_T are the sending end and receiving end voltages, X_T is the net reactance, and X_S is the transfer reactance of the uncompensated line transmission line. Power transfer capability can be increased by adding a series capacitor, followed by a reduction in total reactance X_T [12].

Therefore, net reactance would be

$$X_T = (X_S - X_C), \tag{2}$$

where X_C is the capacitive reactance of the series capacitor.

If the percentage of compensation is K_C, then

$$X_T = (1 - K_C)X_S. \tag{3}$$

[1] Department of Electrical Engineering, Delhi Technological University, India.
[2] Department of Electrical Engineering, Government Engineering College, Siwan, India.
E-mail: neevatika_2k18phdee04@dtu.ac.in, narendra.kumar@dtu.ac.in

DOI: 10.59277/RRST-EE.2026.2.12

The compensation degree (K_C), which ranges from 0 to 100 percent, is described as follows,

$$K_C = \left(\frac{X_C}{X_S}\right) * 100\%, \quad (4)$$

The degree of compensation can theoretically reach 100%, but such high levels may cause excessive currents during disturbances due to subsynchronous resonance, affecting protection and voltage stability. In practice, it is limited to about 80%, with modern systems typically operating at around 50% [13].

The electrical resonance frequency (f_r) for the radial compensated network can be given as

$$f_r = f_s\sqrt{X_C/X_S}, \quad (5)$$

where f_s is the rated frequency of the system, X_S is the total transfer reactance of the network.

The current in a compensated network flows through the machine's armature winding and, when interacting with the turbine-generator shaft, produces subsynchronous and supersynchronous harmonics. It contains the fundamental component along with additional frequency components determined by system and line parameters [12];

$$i(t) = K_c[X\sin(\omega_1 t + \varphi_1) + \\ +Ye^{-\zeta\omega_2 t}\sin(\omega_2 t + \varphi_2)], \quad (6)$$

where damping ratio is symbolised as ζ for the network and can be defined as

$$\zeta = R/2\sqrt{C/L}, \quad (7)$$

ω_2 is the damping frequency, which can be defined as

$$\omega_2 = \omega_n\sqrt{1-(\zeta)^2}, \quad (8)$$

undamped frequency can be defined as

$$\omega_n = \sqrt{1/LC}. \quad (9)$$

The armature current generates electromagnetic torque on the turbine-generator shaft. As it contains subsynchronous and supersynchronous components, their interaction with the system's natural torsional frequency can cause oscillations, leading to mechanical stress and possible failure of the shaft and connected equipment [12].

Although SSR originates from generator–network interactions, its subsynchronous components propagate through the network and appear at multiple nodes, including transformer terminals. As a result, transformers experience voltage waveforms with both fundamental and subsynchronous components, affecting excitation and potentially causing flux buildup and core saturation.

Therefore, understanding SSR characteristics is essential for analyzing its impact on transformer behavior.

3. STUDY SYSTEM

For detailed analysis, this study considers a long transmission line with series compensation to enhance power transfer capability. The system is inspired by the Hydro-Québec 735 kV network in Quebec, which uses series compensation to transmit power from the James Bay region to load centers. Although simplified, it retains key features such as the 735 kV voltage level, 600 km line length, and typical series-compensated radial configuration.

As shown in Fig. 1, the system is modeled as a single-line diagram of a 3-phase, 60 Hz, 735 kV transmission line under weak load conditions. The 600 km line transmits power from a generating station with six 350 MVA units to the receiving end and is divided into two 300 km segments connected by buses B1, B2, and B3. Each segment has 30% series compensation to enhance power transfer, along with a 330 Mvar shunt reactor for compensation on both lines.

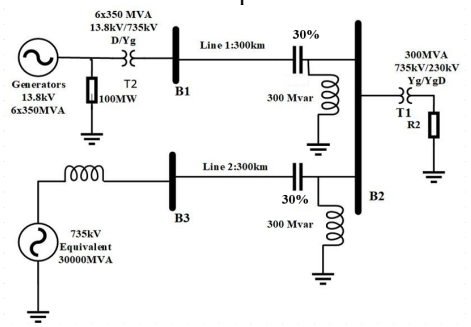

Fig. 1− The single line diagram of a power system.

3.1 MATLAB/SIMULINK IMPLEMENTATION

The system in Fig. 1 is implemented in MATLAB/Simulink (R2021a) using the Simscape Electrical toolbox. Fig. 2 shows the detailed Simulink model, which includes: a generator subsystem (six 350 MVA synchronous machines), a 13.8/735 kV, 300 MVA step-up transformer, two 300 km transmission line segments (distributed parameter model), 30% series-compensated capacitor banks, 330 Mvar shunt reactors at both ends, a three-phase fault breaker with programmable timing, measurement blocks (voltage, current, flux, power), and circuit breaker control logic. All system parameters used in the model are listed in Table 1 in appendices section.

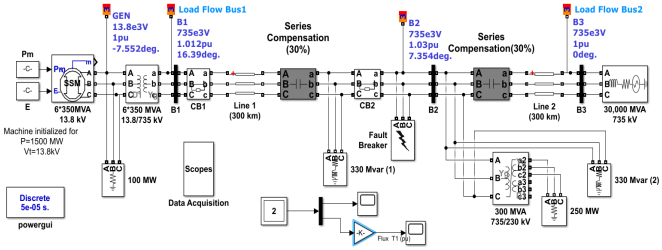

Fig. 2 − MATLAB/Simulink implementation of the studied system.

4. MATHEMATICAL MODELING

4.1 TRANSFORMER FLUX DYNAMICS AND SATURATION CONDITION

The core flux $\phi(t)$ is governed by Faraday's law of induction, integrating the terminal voltage $v(t)$ [14,15]:

$$\phi(t) = \frac{1}{N}\int v(t)dt. \quad (10)$$

For a voltage comprising fundamental (f_s = 60 Hz) and subsynchronous components [12]

$$v(t) = \sqrt{2}V_S\sin(2\pi f_s t) + \sqrt{2}V_{SSR}\sin(2\pi f_{SSR}t), \quad (11)$$

where, V_S, V_{SSR} and f_{SSR} are the magnitude of the fundamental voltage component, the magnitude of the subsynchronous voltage component, and the subsynchronous frequency, respectively.

The flux becomes:

$$\phi(t) = \underbrace{\frac{V_S}{2\pi f_s}[1-\cos(2\pi f_s t)]}_{\phi_{fund(t)}} + \underbrace{\frac{V_{SSR}}{2\pi f_{SSR}}[1-\cos(2\pi f_{SSR}t)]}_{\phi_{SSR(t)}}, \quad (12)$$

where $\phi_{fund(t)}$ is the flux component due to fundamental voltage, and $\phi_{SSR(t)}$ is the flux component due to subsynchronous voltage.

The worst-case peak flux (ϕ_{peak}) occurs when

fundamental and SSR components align in phase:

$$\phi_{peak} = \frac{V_S}{2\pi f_s} + \frac{V_{SSR}}{2\pi f_{SSR}}. \quad (13)$$

Expressed in per-unit (pu) relative to nominal flux ($\phi_{base} = \frac{V_{base}}{2\pi f_s}$)

$$\phi_{peak} = V_S^{pu} + V_{SSR}^{pu}\frac{f_s}{f_{SSR}}, \quad (14)$$

Transformer saturation occurs when the magnetic flux $\phi(t)$ exceeds the material-specific knee-point flux ϕ_{sat}, beyond which the magnetizing inductance sharply reduces. The saturation condition is mathematically expressed as [16]:

$$\phi_{peak} > \phi_{sat}, \quad (15)$$

where ϕ_{sat} is the saturation knee point (typically 1.15–1.28 pu). The saturation severity is quantified by the excess flux ratio:

$$\gamma = \frac{\phi_{peak}}{\phi_{sat}} - 1, \quad (16)$$

where γ the excess flux ratio (dimensionless) indicates how far beyond saturation the flux extends (γ = 0 at saturation threshold, γ > 0 indicates saturation).

Under saturation, magnetizing current $i_m(t)$ exhibits piecewise behavior [15]:

$$i_m(\phi) = \begin{cases} \frac{\phi}{L_m}, & \phi \le \phi_{sat} \\ \frac{\phi_{sat}}{L_m} + k(\phi - \phi_{sat})^7, & \phi > \phi_{sat} \end{cases} \quad (17)$$

where k is the saturation coefficient (0.1–0.3 pu) – determines the steepness of the saturation characteristic, ϕ is the instantaneous flux, L_m is the unsaturated magnetizing inductance, and ϕ_{sat} is the saturation knee point flux.

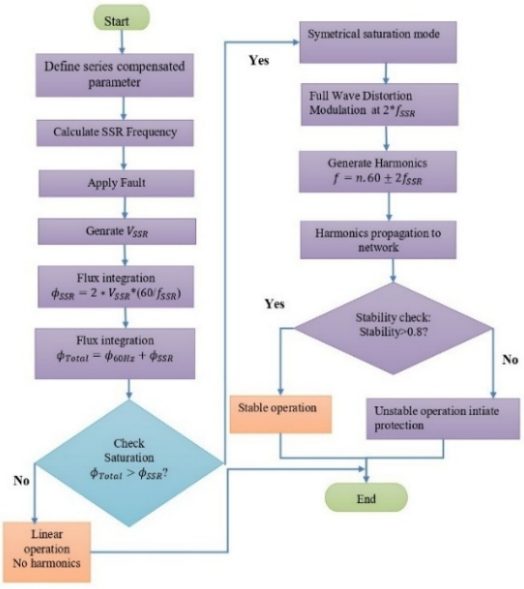

Fig. 3 − The workflow for transformer saturation and stability assessment during faults.

This model captures the essential features of both linear magnetization and the nonlinear saturation region and is implemented using a lookup-table-based core characteristic. Figure 3 illustrates the detailed computational workflow for saturation assessment. The workflow in Fig. 3 is implemented in MATLAB/Simulink through a sequential simulation. The system is first initialized at steady state, followed by the application of a three-phase fault at a specified bus. Transformer terminal voltage is recorded during and after fault clearing, and core flux is obtained by integrating the voltage (Faraday's law). This flux is compared with the saturation knee point, activating a lookup table-based nonlinear magnetization model when exceeded. The corresponding magnetizing current is then computed, and FFT is applied to the voltage and current waveforms to extract frequency components, enabling analysis of SSR interaction, flux dynamics, and saturation behavior.

4.1 DEMODULATION DUE TO TRANSFORMER SATURATION

The flux waveform enters the saturation region when its magnitude exceeds the saturation threshold ϕ_{sat}. Beyond this point, the magnetizing current becomes nonlinear [17]. Let $i_m(t)$ represent the magnetizing current, which under saturation becomes a nonlinear function of flux, $i_m = f_{NL}(\phi)$. For analytical approximation, consider a Taylor series expansion:

$$i_m(t) = a_1\phi(t) + a_2\phi^2(t) + a_3\phi^3(t) + \cdots . \quad (18)$$

Here a_1, a_2, a_3 are the nonlinear terms (quadratic and cubic) that introduce harmonic and intermodulation components due to trigonometric product identities. We now analyze how frequency components mix under the square and cube of $\phi(t)$ [17],

$$\phi(t) \approx A\cos(2\pi f_1 t) + B\cos(2\pi f_{SSR} t). \quad (19)$$

Squaring eq. (19), we get

$$\phi^2(t) = A^2\cos^2(2\pi f_1 t) + +2AB\cos(2\pi f_1 t)\cos(2\pi f_{SSR} t) + B^2\cos^2(2\pi f_{SSR} t). \quad (20)$$

Using

$$\cos(a)\cos(b) = \frac{1}{2}[\cos(a+b) + \cos(a-b)], \quad (21)$$

$$\cos^2(x) = \frac{1}{2}[1 + \cos(2x)], \quad (22)$$

we get $\phi^2(t)$ at the following frequencies: (i) DC (0 Hz), $2f_1$; (ii) $2f_{SSR}$; (iii) $f_1 + f_{SSR}$, $f_1 - f_{SSR}$.

Thus, the quadratic term introduces sidebands and $f_1 \pm f_{SSR}$. Similarly, the cubic term $\phi^3(t)$ introduces the following terms: $f_1 \pm 2f_{SSR}, 3f_1, 3f_{SSR}, etc.$

Hence, the full spectrum of the magnetizing current contains:

- Fundamental: $f_1 = 60$ Hz
- Sidebands: $f_1 \pm f_{SSR}$, $f_1 \pm 2f_{SSR}$
- Harmonics: $2f_1$, $3f_1$,….
- Modulated harmonics: $2f_1 \pm f_{SSR}$, $3f_1 \pm f_{SSR}$,…

This phenomenon is analogous to amplitude modulation, where a high-frequency carrier f_1 is modulated by a low-frequency signal f_{SSR} [9]. Transformer saturation acts as a nonlinear demodulator, converting SSR oscillations into amplitude variations in the magnetizing current and its harmonics, effectively behaving as a frequency mixer that generates sidebands and spreads energy across the spectrum.

These sidebands can degrade power quality, disrupt protection schemes, and cause relay maloperation due to harmonic sensitivity. They also violate the sinusoidal steady-state assumptions used in many control designs and impedance-based models [18,19].

5. SIMULATION RESULTS AND CASE STUDIES

5.1 FREQUENCY RESPONSE ANALYSIS OF THE SYSTEM MODEL

Impedance–frequency analysis is a key tool for assessing

power system dynamics, helping identify resonance points influenced by line, generation, and load characteristics. In series-compensated systems, subsynchronous modes appear as impedance zeros and poles below the nominal frequency. If a turbine-generator torsional mode aligns with an impedance zero, the corresponding pole can amplify voltages and potentially cause transformer core saturation.

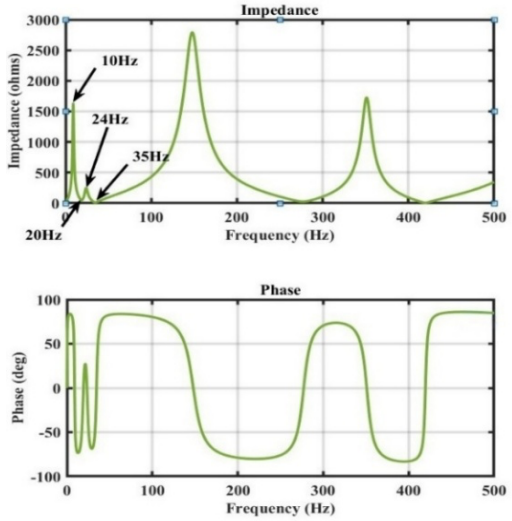

Fig. 4 – The positive sequence impedance versus frequency characteristics of a series compensated power system at 30% of series compensation.

The Thevenin positive impedance at bus 2 (Fig. 4) shows the system's magnitude and phase response, with key resonances as follows:

- *Series resonance* (20 Hz): due to the interaction between the line inductance and the series capacitors, it varies with the compensation level.
- *Parallel resonance* (10 Hz): caused by shunt reactors and series compensation, producing impedance peaks.
- *Distributed parameter resonance:* arises from the long (600 km) line's inductance and capacitance, often excited during fault clearing.

These resonance modes critically affect system performance under fault conditions, particularly with respect to SSR and transformer saturation.

5.2 TIME-DOMAIN SIMULATIONS

To evaluate the impact of SSR on transformer saturation and voltage modulation, a detailed simulation is conducted. The test system includes a 300 MVA, 735/230 kV transformer (T_1) energized from the high-voltage side via a 13.8 kV, 300 km transmission line with two parallel circuits, each having 30% fixed series compensation. A three-phase fault is applied on line 2 at bus B_2 for three cycles (0.05 s). The study examines transformer flux and magnetizing current under subsynchronous excitation during and after fault clearing.

5.2.1 CASE 1: SATURATION OF TRANSFORMER

Figure 5,a shows the fault current waveform I_a, with a sharp rise during the fault and a complex recovery afterward. The A-phase voltage at bus B_2 [Fig. 5(b)], reveals a 10 Hz subsynchronous oscillation immediately after fault clearance, confirmed by the spectrum in Fig. 5(c). This 10 Hz component, superimposed on the 60 Hz fundamental, causes cumulative flux buildup in the transformer core.

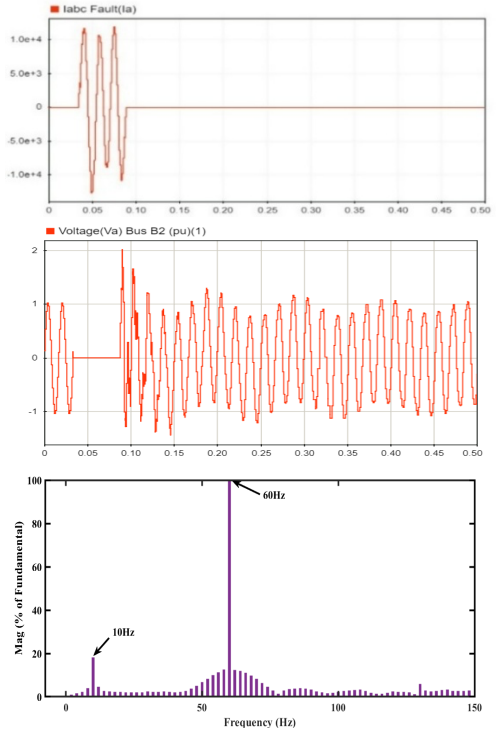

Fig. 5 – (a) Three-phase line to ground fault current at line 2; (b) Bus voltage at B2, and (c) Frequency spectrum of bus voltage of phase A.

Although the voltage magnitude recovers post-fault, the low-frequency oscillation drives the flux beyond the linear region into saturation. As seen in Fig. 6,a, the flux reaches 1.89 pu, exceeding the saturation knee point (1.28 pu). The magnetizing current in Fig. 6(b) shows symmetrical pulses, indicating saturation in both positive and negative flux directions.

5.2.2 CASE 2: VOLTAGE MODULATION

The symmetrical saturation causes strong modulation in the magnetizing current and terminal voltage.

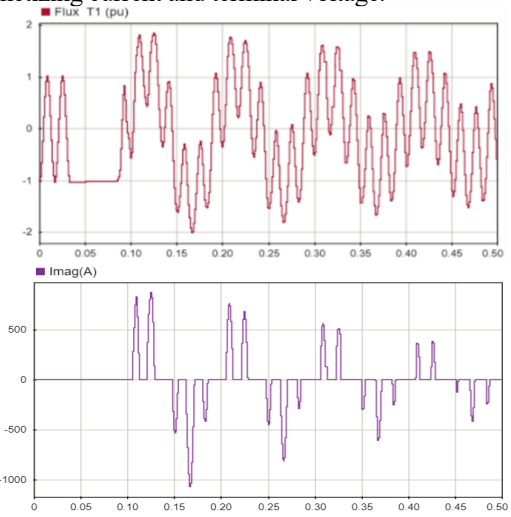

Fig. 6 –Impact of transformer saturation at a subsynchronous frequency:(a) Transformer core flux (b) Transformer magnetizing current.

Figure 7,a shows the magnetizing current spectrum, which includes:

- Sidebands at 40 Hz and 80 Hz, resulting from 20 Hz modulation of the 60 Hz waveform. These originate from the half-period pulse trains caused by the 10 Hz flux oscillation.

- Odd harmonics (*e.g.*, 3rd, 5th, 7th) are also modulated at 20 Hz, introducing amplitude-modulated spectral features.
- Even harmonics arise from residual waveform asymmetries and are modulated at 10 Hz, as evidenced by new components at 110 Hz (120 − 10 Hz) and 130 Hz (120 + 10 Hz).

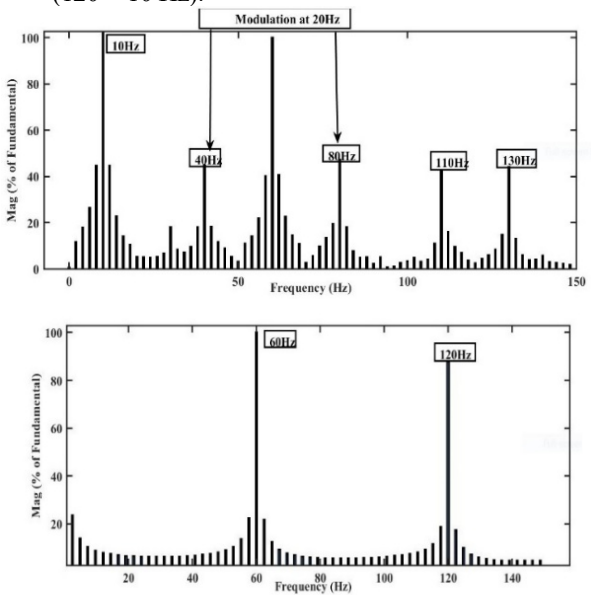

Fig. 7 − The impact of transformer saturation at a subsynchronous frequency: (a)Frequency spectrum of magnetizing current with series compensated, and (b)Without series compensation.

This demonstrates the complex harmonic and intermodulation behavior caused by transformer saturation under subsynchronous excitation. In contrast, Fig. 7 b shows the magnetizing current spectrum without series compensation; although harmonics exist, no sidebands appear, confirming that series compensation intensifies nonlinearity and introduces spectral broadening. Figure 8 compares the two cases, highlighting that series-compensated systems are more prone to deep saturation and spectral distortion, thereby increasing the risk of instability and insulation stress.

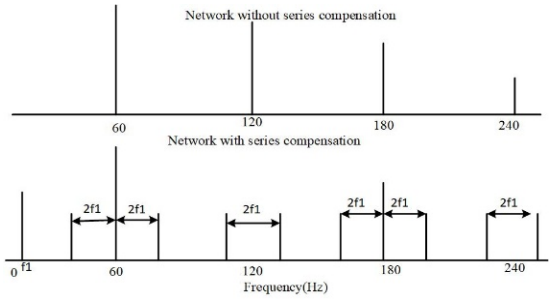

Fig. 8 − The magnetizing current spectrum of the transformer during fault clearing, with and without series compensation (SSR at f_1).

5.2.3 CASE 3: EFFECT OF SERIES COMPENSATION LEVEL

A systematic analysis was performed for compensation levels from 0% to 80% to understand how series compensation influences transformer saturation risk. Fig. 9 shows how the two critical resonance frequencies vary with compensation. Two fundamental frequencies govern the system behavior:

- *Series resonance frequency*: $f_{series} = 60\sqrt{K_c}$, — decreases from 26.8 Hz at 20% compensation to 13.4 Hz at 50% compensation.
- *Shunt resonance frequency:* $f_{shunt} = 10/\sqrt{K_c}$ — decreases from 22.36 Hz at 20% compensation to 14.14 Hz at 50% compensation.

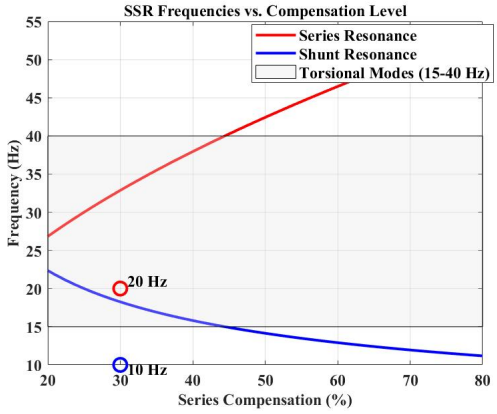

Fig. 9 − SSR frequencies vs. compensation showing dangerous 20 Hz/10 Hz resonances at 30% compensation (torsional zone: gray).

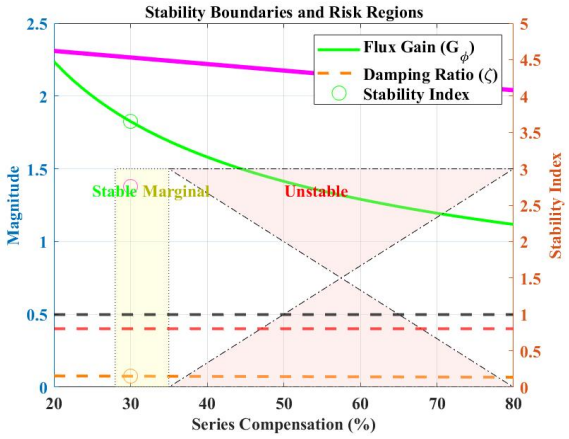

Fig. 10 − The stability thresholds vs. compensation. 30% case (marked) in marginal zone with flux gain >1.25 and damping ratio near instability limit.

As these frequencies decrease, two effects combine to increase transformer saturation risk:

- *Flux amplification*: from eq. (14), the flux gain factor is $G_\phi = 1/\sqrt{K_c}$. Lower SSR frequencies mean higher flux gain—a given SSR voltage produces larger flux excursions.
- *Reduced damping*: higher compensation reduces system damping, according to ($\zeta = 0.08 - 0.015K_c$), allowing oscillations to persist longer.

For the 30% compensation case study (K_C = 0.3, index = 0.86), the 20 Hz series resonance coincides with turbo-generator Mode 2 (18-22 Hz), while the 10 Hz shunt resonance induces saturation at remarkably low disturbance voltages (0.014 pu). This configuration exhibits only 14% stability margin, with fault-clearing events generating flux peaks up to 3.4 pu (266% above the saturation knee). Critically, the SSR-stability relationship exhibits strong nonlinearity: Beyond 35% compensation, every 1% increase reduces the stability index by 8.2% while boosting flux gain by 1.4%. To ensure secure operation, compensation should be limited to 28% (K_C = 0.28), maintaining frequencies above 25 Hz and a damping ratio $\zeta >$ 0.05. For existing 30% compensated systems, mitigation requires 20 Hz notch filtering and flux-based control interventions at $\phi > 1.20\phi_{sat}$. These findings establish 35%

compensation as an absolute upper limit – beyond which SSR-induced saturation leads to uncontrollable voltage collapse, regardless of control system enhancements.

6. **CONCLUSION**

This paper presents a comprehensive analysis of transformer saturation under subsynchronous resonance in series-compensated systems, highlighting a nonlinear effect often overlooked in classical SSR studies. The key conclusions are:

- Subsynchronous resonance (5–15 Hz) can cause transformer core saturation even with low SSR voltage magnitudes, as interaction with the 60 Hz fundamental leads to significant flux excursions.
- Series compensation lowers SSR frequency, increasing its overlap with transformer dynamics; greater compensation results in deeper, more sustained saturation.
- Saturation produces distorted voltage and current waveforms, including pulse-like magnetizing currents, subharmonics, and intermodulation sidebands (*e.g.*, 40 Hz, 80 Hz, 110 Hz, 130 Hz), affecting power quality and protection.

These results highlight the need to account for nonlinear transformer behavior in SSR analysis, particularly in modern grids with high series compensation and long transmission lines. Future work can focus on real-time SSR detection, hardware-based saturation control, and damping using grid-scale energy storage.

CREDIT AUTHORSHIP CONTRIBUTION STATEMENT

NEEVATIKA VERMA: Conceptualization, methodology, writing – original draft, data curation, software

NARENDRA KUMAR: Formal analysis, supervision, validation, writing – review, and editing.

APPENDICES

Table 1

System parameter

Component	Parameter	Value
Generator (each of six)	Rated power	350 MVA
	Rated voltage	13.8 kV
	Frequency	60 Hz
Transformer T_1	Rated power	300 MVA
	Voltage ratio	735/230 kV
	Winding resistance (primary)	0.002 pu
	Winding resistance (secondary)	0.002 pu
	Leakage inductance	0.08 pu
	Magnetizing inductance (unsaturated)	500 pu
	Saturation knee point	1.28 pu
	Saturation coefficient (k)	0.15 pu
Transmission line (per segment, 300 km)	Positive sequence resistance	0.023 Ω/km
	Positive sequence inductance	0.93 mH/km
	Positive sequence capacitance	12.7 nF/km
Series compensation (30%)	Capacitor bank (each line)	42.8 μF
Shunt reactor (each line)	Reactive power	330 Mvar
	Inductance	5.2 H

Received on 11 July 2025

REFERENCES

1. M. Gavrilas, R. Toma, *Flexible alternating current transmission system optimization in the context of large disturbance voltage stability*, Rev. Roum. Sci. Techn. – Électrotechn. et Énerg., **66**, *1*, pp. 21–26 (2021).
2. A.H.A.N. Nawas, S. Sundaramoorthy, *Giant trevally optimized congestion management using FACTS controller allocation in deregulated electricity markets*, Rev. Roum. Sci. Techn. – Électrotechn. et Énerg., **69**, *4*, pp. 377–382 (2024).
3. S. Arockiaraj, B.V. Manikandan, A. Bhuvanesh, *Fuzzy logic controlled STATCOM with a series compensated transmission line analysis*, Rev. Roum. Sci. Techn. – Électrotechn. et Énerg., **68**, *3*, pp. 307–312 (2023).
4. N. Verma, N. Kumar, S. Gupta, H. Malik, F. Pedro, G. Márquez, *Review of sub-synchronous interaction in wind integrated power systems: classification, challenges, and mitigation techniques*, Prot. Control Mod. Power Syst., **8**, *2*, pp. 1–26 (2023).
5. S. Rezaei, *Behavior of protective relays during subsynchronous resonance in transmission line and adaptation of generator out-of-step protection*, IEEE Transactions on Industry Applications, **55**, *6*, pp. 5687–5698 (2019).
6. E. Hajipour, M. Vakilian, M. Sanaye-Pasand, *Current-transformer saturation prevention using a controlled voltage-source compensator*, IEEE Trans. Power Deliv., **32**, *2*, pp. 1039–1048 (2016).
7. H. Wang, Y. Wang, X. Xiao, Z. Ma, Q. Xu, *Harmonic state space based stability analysis of LCC-HVDC system with saturated transformer*, IEEE Trans. Power Deliv., pp. 1–10 (2025).
8. H Z. Weng, S. Wang, X. Lin, L. Chen, J. Huang, and Z. Li, *Waveform similarity-based transformer phase differential protection against current transformer saturation*, Autom. Electr. Power Syst., **43**, *4*, pp. 132–138 (2019).
9. J. Berge, R.K. Varma, *Determination of the spectrum of frequencies generated by a saturated transformer*, 2011 24th Canadian Conference on Electrical and Computer Engineering (CCECE), Canada, pp. 1272–1277 (2011).
10. A. Dash, M.K.K. Mohanta, D. De, P. Abhishek, A. Castellazzi, *Modeling and mitigation of transformer saturation in dual-active-bridge converter*, 2021 IEEE 12th Energy Conversion Congress & Exposition-Asia (ECCE-Asia), Singapore, pp. 408–413 (2021).
11. S.-F. Chou, X. Wang, F. Blaabjerg, *Subsynchronous resonance analysis in multi-bus multi-VSC power system based on two-port network modeling method*, 2020 IEEE Energy Conversion Congress and Exposition (ECCE), USA, pp. 5696–5702 (2020).
12. K.R. Padiyar, *Analysis of subsynchronous resonance in power systems*, Springer US, pp. 1–300 (1999).
13. N. Verma, N. Kumar, *DFIG-based wind plant coupled series compensated transmission line: modeling and SSR stability analysis*, J. Inst. Eng. Ser. B, **103**, *6*, pp. 1917–1926 (2022).
14. C.-M. Gheorghe, I.-A. Macinic, A.-G. Gheorghe, *Oblong core cross-section impact on power transformer characteristics*, Rev. Roum. Sci. Techn. – Électrotechn. et Énerg., **67**, *3*, pp. 281–286 (2022).
15. S. Abdulsalam, X. Wilsun, W.L.A. Neves, L. Xian, *Estimation of transformer saturation characteristics from inrush current waveforms*, IEEE Power Eng. Soc. Gen. Meet. PES, **21**, *1*, pp. 170–177 (2006).
16. M. Dolinar, D. Dolinar, Š. Gorazd, B. Polajžer, J. Ritonja, *A three-phase core-type transformer iron core model with included magnetic cross saturation*, IEEE Trans. Magn., **42**, *10*, pp. 2849–2851 (2006).
17. I. Daut, S. Hasan, S. Taib, *Magnetizing current, harmonic content and power factor as the indicators of transformer core saturation*, J. Clean Energy Technol., **1**, *4*, pp. 304–307 (2013).
18. M. Fritsch, M. Wolter, *Saturation of high-frequency current transformers: challenges and solutions*, IEEE Trans. Instrum. Meas., **72**, pp. 1–10 (2023).
19. R. Elumalai, R. Varadhan, *Intelligent controller-based dynamic voltage restorer to reduce the voltage fluctuations*, Rev. Roum. Sci. Techn. – Électrotechn. et Énerg., **71**, *1*, pp. 21–26 (2026).